Hindawi Publishing Corporation
Journal of Nanomaterials
Volume 2013, Article ID 101508, 6 pages
http://dx.doi.org/10.1155/2013/101508

Research Article

Applied Pressure on Altering the Nano-Crystallization Behavior of $Al_{86}Ni_6Y_{4.5}Co_2La_{1.5}$ Metallic Glass Powder during Spark Plasma Sintering and Its Effect on Powder Consolidation

X. P. Li,[1] M. Yan,[1] G. Ji,[2] and M. Qian[1]

[1] *The University of Queensland, School of Mechanical and Mining Engineering, ARC Centre of Excellence for Design in Light Metals, Brisbane, QLD 4072, Australia*
[2] *Unité Matériaux et Transformations, UMR CNRS 8207, Université Lille 1, Bâtiment C6, 59655 Villeneuve d'Ascq, France*

Correspondence should be addressed to M. Yan; m.yan2@uq.edu.au

Received 19 December 2012; Accepted 25 January 2013

Academic Editor: Jianxin Zou

Metallic glass powder of the composition $Al_{86}Ni_6Y_{4.5}Co_2La_{1.5}$ was consolidated into 10 mm diameter samples by spark plasma sintering (SPS) at different temperatures under an applied pressure of 200 MPa or 600 MPa. The heating rate and isothermal holding time were fixed at 40°C/min and 2 min, respectively. Fully dense bulk metallic glasses (BMGs) free of particle-particle interface oxides and nano-crystallization were fabricated under 600 MPa. In contrast, residual oxides were detected at particle-particle interfaces (enriched in both Al and O) when fabricated under a pressure of 200 MPa, indicating the incomplete removal of the oxide surface layers during SPS at a low pressure. Transmission electron microscopy (TEM) revealed noticeable nano-crystallization of face-centered cubic (fcc) Al close to such interfaces. Applying a high pressure played a key role in facilitating the removal of the oxide surface layers and therefore full densification of the $Al_{86}Ni_6Y_{4.5}Co_2La_{1.5}$ metallic glass powder without nano-crystallization. It is proposed that applied high pressure, as an external force, assisted in the breakdown of surface oxide layers that enveloped the powder particles in the early stage of sintering. This, together with the electrical discharge during SPS, may have benefitted the viscous flow of metallic glasses during sintering.

1. Introduction

Metallic glasses (MGs) have been investigated for decades due to their intrinsically unique physical and chemical properties [1]. Al-based MGs are promising advanced materials which have attracted increasing attention for their ultrahigh specific strength and relatively low cost compared with most other MGs [2]. However, due to their low glass forming ability (GFA), fabrication of Al-based BMGs through a conventional cooling process from liquid has proved to be challenging [3–5]. The first conceptual Al-based BMG with 1 mm diameter was fabricated using a copper mold casting approach in 2009 [6] since the Al-based MG was first reported in 1988 [7] and the alloy reported [6] remains to be the best glass forming Al-based BMG to date. The slow development of Al-based BMGs in terms of their GFA impedes the potential application of these materials.

Since MG powder can be readily prepared by gas-atomization [8], powder metallurgy (PM), especially the spark plasma sintering (SPS) technique, offers an alternative to the fabrication of BMGs. Fully dense Ti-, Ni-, Cu-, and Fe-based BMGs with >10 mm diameters have been fabricated using SPS [9–12]. These MGs have much higher glass transition temperatures (T_g) [1, 3] compared to Al-based MGs and therefore can be readily consolidated at high sintering temperatures without nano-crystallization. As for Al-based BMGs, because their T_g temperatures are generally <300°C, nano-crystallization is easy to occur during SPS. Hence, few studies have succeeded in fabricating fully dense Al-based BMGs without crystallization [13–15]. On the other hand, a previous study [16] has revealed that MG powder is enveloped by an oxide layer which would inhibit viscous flow of the amorphous material for full densification. As a result, it is essential to remove this surface oxide layer to enable viscous

flow for full densification of Al-based MG powder at low temperatures.

It has been proposed [17] that the electrical discharge during SPS has a cleaning effect which can help to remove the surface oxide layers on metallic powders. In general, the higher the heating rate during SPS, the more effective the cleaning effect will be [18]. However, due to the low T_g of Al-based MGs (<300°C), it is difficult to accurately control the temperature rise and avoid overshoot when a very high heating rate (>40°C/min) is used. Consequently, it is necessary to consider employing other options such as the use of high pressure to assist in the breakdown of surface oxide layers that envelope the powder particles. In addition, applying high pressure during SPS is expected to favor the viscous flow between the Al-based MG powder particles for enhanced densification. No study has been reported on looking into the role of applying high pressure during the SPS of Al-based MG powder from these two perspectives.

In this study, a 10 mm diameter (Φ10 mm) $Al_{86}Ni_6Y_{4.5}Co_2La_{1.5}$ BMG was fabricated using SPS. The influence of applied pressure on the densification of $Al_{86}Ni_6Y_{4.5}Co_2La_{1.5}$ MG powder was investigated through detailed characterization of the as-sintered samples using scanning electron microscopy (SEM) and transmission electron microscopy (TEM) by focusing on selected particle-particle interfaces. The underlying reasons were discussed.

2. Experimental Procedure

Nitrogen-gas-atomized $Al_{86}Ni_6Y_{4.5}Co_2La_{1.5}$ MG powder was used. To ensure a fully amorphous state, only powder particles that are finer than 25 μm in diameter were used based on a previous study of the powder [8, 17]. The amorphous nature of the selected powder was further confirmed by X-ray diffraction (XRD) (D/max III, CuK_α target, operated at 40 kV and 60 mA).

The surfaces of the starting powder were studied using X-ray photoelectron spectroscopy (XPS) (Kratos Axis ULTRA XPS, monochromatic Al X-ray, C 1 s at 285 eV was used as a standard). XPS survey scans were taken at an analyzer pass energy level of 160 eV and carried out over the binding energy range of 1200-0 eV with 1.0 eV steps and 100 ms dwell time at each step. The base pressure in the analysis chamber was maintained in the range of 1.33×10^{-7} Pa to 1.33×10^{-6} Pa during analysis.

The SPS experiments were conducted on an SPS-1030 made by SPS SYNTEX INC, Japan. A tungsten carbide (WC) die (outer diameter 30 mm, inner diameter 10 mm, and height 20 mm) was used. The T_g temperature of the $Al_{86}Ni_6Y_{4.5}Co_2La_{1.5}$ MG powder varies with heating rate and was recorded to be 270°C at 40°C/min in argon [8]. To avoid temperature overshoot and maximize the cleaning effect of SPS, the heating rate was fixed at 40°C/min, based on a few preliminary heating trials with the SPS machine. The isothermal holding time was fixed to be 2 min. To study the influence of sintering temperature and pressure on the densification of the $Al_{86}Ni_6Y_{4.5}Co_2La_{1.5}$ MG powder, a range of sintering temperatures was chosen, 248.5, 258.5, 268.5, 278.5, 288.5, 298.5, and 308.5°C. The pressure applied was 200 MPa or 600 MPa. Table 1 summarizes the sintering parameters used.

Table 1: SPS experimental parameters used for this study.

Sintering temperature (°C)	248.5	258.5	268.5	278.5	288.5	298.5	308.5
Pressure (MPa)	200, 600			200			
Holding time (min)	2						
Heating rate (°C/min)	40						

The sintered density was measured using the Archimedes method. The SPS-processed samples were cut, ground, and polished. They were then characterized using SEM (JEOL 7001F, accelerating voltage 15 kV and working distance 10 mm) and TEM (JEOL JEM 2100, operated at 200 kV), where the TEM samples were prepared using a precision ion polishing system (Gatan's PIPS, operated at −50°C).

3. Results and Discussion

Figure 1(a) shows the morphology of the starting powder and the XPS results are shown in Figure 1(b). Strong oxide signals are detected on the MG powder surfaces, consistent with the observations reported by Yan et al. [16]. An SPS-processed 10 mm diameter $Al_{86}Ni_6Y_{4.5}Co_2La_{1.5}$ BMG sample (4 mm in height) is shown in Figure 1(c), which was fabricated by heating the powder to 248.5°C at 40°C/min and held at temperature for 2 min under 600 MPa. The XRD results shown in Figure 1(c) indicate that the as-sintered $Al_{86}Ni_6Y_{4.5}Co_2La_{1.5}$ BMG is essentially amorphous.

Figure 2 shows the density of SPS-processed $Al_{86}Ni_6Y_{4.5}Co_2La_{1.5}$ BMGs achieved at different sintering temperatures and pressures. Under an applied pressure of 200 MPa, the density of the BMGs increased with increasing sintering temperature from 248.5°C to 278.5°C. But further increasing the sintering temperature to 308.5°C, which is above the T_g of the alloy and also above the peak temperature for the first crystallization stage of the $Al_{86}Ni_6Y_{4.5}Co_2La_{1.5}$ MG powder [8], resulted in little increase in the sintered density. In contrast, increasing the applied pressure from 200 MPa to 600 MPa led to a substantial increase in the sintered density at each of the three temperatures tested. Increasing pressure was much more effective than increasing sintering temperature. This implies that sintering pressure plays a key role in the densification of $Al_{86}Ni_6Y_{4.5}Co_2La_{1.5}$ MG powder during SPS. In fact, the near full density achieved by increasing pressure is difficult to achieve by increasing sintering temperature alone without nano-crystallization. To find out the underlying reasons for this big difference, the as-sintered microstructure was analyzed in detail using SEM and TEM, with a special focus being placed on the interfaces between powder particles.

X-ray mapping was applied to all the constituent elements (i.e., Al, Ni, Y, Co, and La) as well as O in the samples that

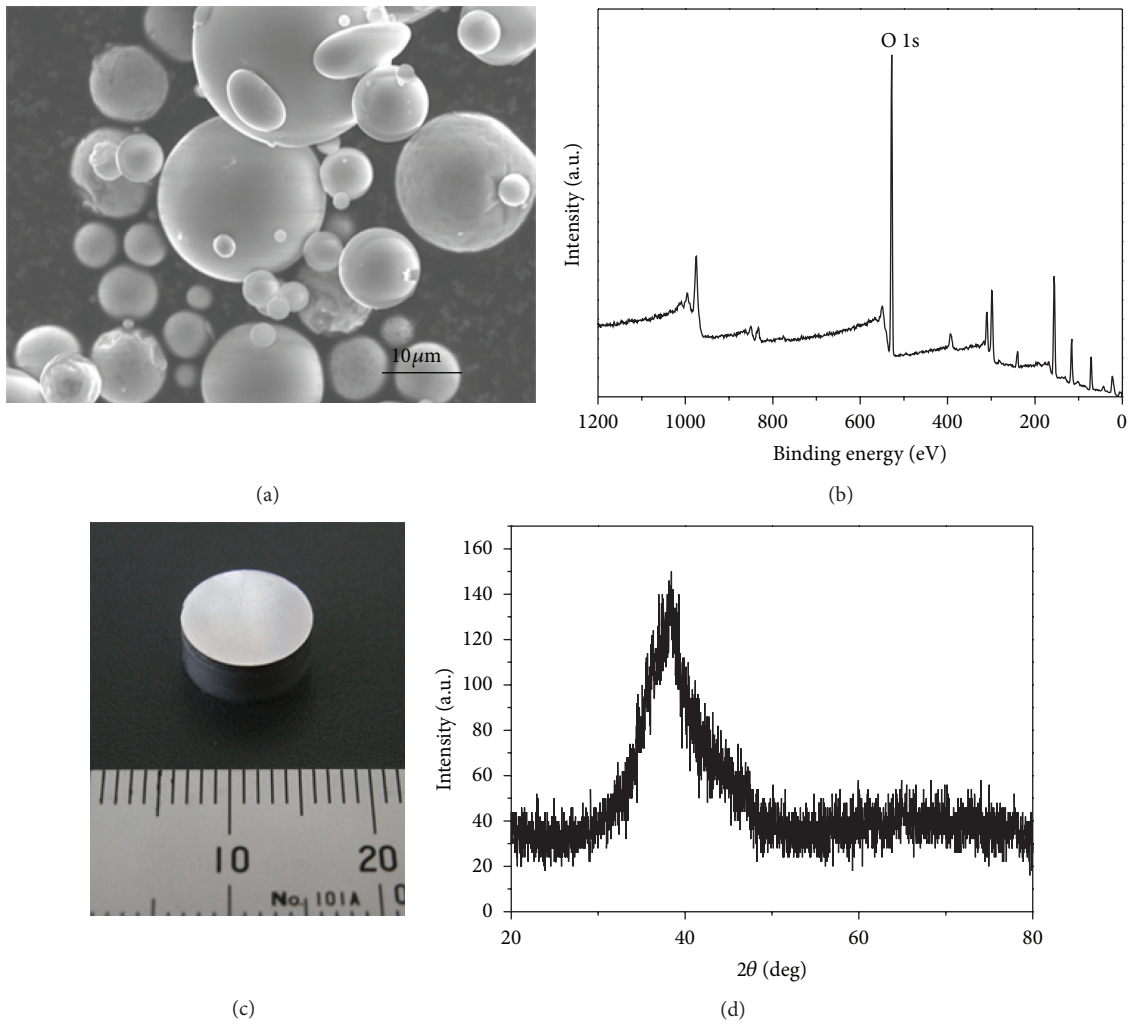

FIGURE 1: (a) SEM image of the starting $Al_{86}Ni_6Y_{4.5}Co_2La_{1.5}$MG powder used for fabrication; (b) XPS survey spectra of the $Al_{86}Ni_6Y_{4.5}Co_2La_{1.5}$ MG powder; (c) a 10 mm diameter $Al_{86}Ni_6Y_{4.5}Co_2La_{1.5}$ BMG disk (thickness: 4 mm) (sintering conditions: 2 min at 248.5°C under 600 MPa); and (d) XRD pattern of the fabricated $Al_{86}Ni_6Y_{4.5}Co_2La_{1.5}$ sample.

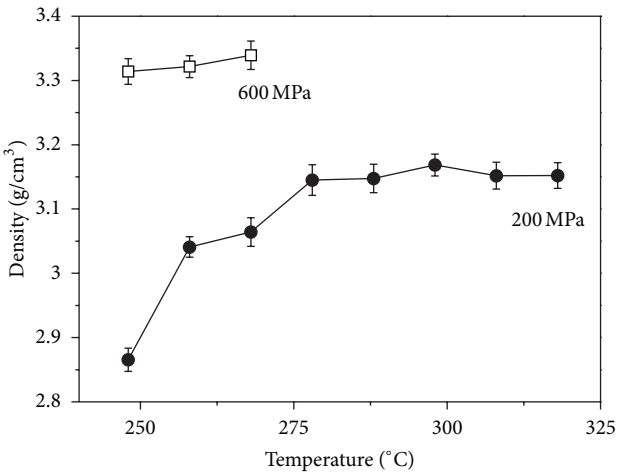

FIGURE 2: Sintered densities of the SPS-processed samples as a function of SPS sintering temperature and pressure.

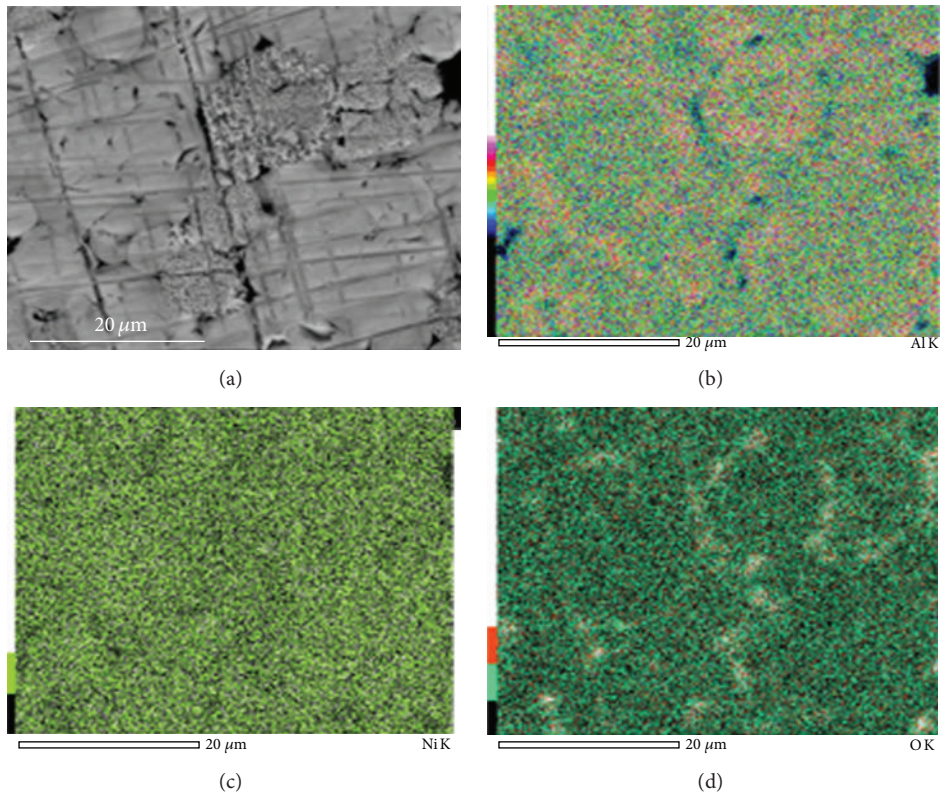

Figure 3: SEM mapping results of Al and Ni as well as O in a selected area of an SPS-processed sample sintered at 248.5°C for 2 min under 200 MPa. The distribution of Y, Co, and La is generally homogeneous and similar to that of Ni.

were sintered at 248.5°C under 200 MPa. Figure 3 shows the results of Al, Ni, and O. The distribution of Ni, Y, Co, and La is homogenous in the microstructure, showing few features. However, Al and O are clearly enriched in areas close to the initial particle-particle interfaces (see Figures 3(b) and 3(d)). Furthermore, these Al- and O-enriched areas underwent only limited sintering, where the sintering necks are still recognizable between neighboring particles (see Figure 3(a)), compared to those well-sintered oxygen-deficient areas. It can be deduced that the surface oxide layers have hindered the densification process of the $Al_{86}Ni_6Y_{4.5}Co_2La_{1.5}$ MG powder during SPS, and that the 200 MPa of applied pressure can only ensure limited removal of these oxide surface layers. To confirm this inference, TEM was used to investigate the interfaces between the particles in the SPS-processed sample, and the results are shown in Figures 4 and 5.

Figure 4(a) shows that the interface between two particles in the same SPS-processed sample (sintered at 248.5°C under 200 MPa) has undergone noticeable crystallization. The interface layer is about 50 nm thick and oxygen can be detected at the interface using TEM energy dispersive X-ray (EDX) (see Figure 4(c)). This further confirms that the oxide surface layers were not completely removed during SPS under the applied pressure of 200 MPa. In contrast, clean interfaces between particles were uniformly observed in the SPS-processed samples under an applied pressure of 600 MPa. An example is shown in Figure 4(b).

Figure 5(a) shows a detailed view of the aforementioned crystallized interface area (Figure 4(a)) together with the surrounding amorphous matrix. Based on the selected area electron diffraction (SAED) patterns (inset in Figure 5(a)), these crystallized phases are indexed to be fcc-Al. Figure 5(b) shows a high-resolution TEM image of these fcc-Al nanocrystals which are about 10 nm in size. In contrast, no crystallization was detected in samples that were sintered at the same temperature (248.5°C) but under 600 MPa (see Figure 4(b)). The difference can be explained below. Under an applied pressure of 200 MPa and a heating rate of 40°C/min, it is difficult to completely remove the surface oxide layers on powder particles, as evidenced by the results shown in Figures 3 and 4. The remaining oxide surface layers prevent viscous flow between the powder particles and therefore inhibit full densification. Consequently, the sintering necks between the neighboring particles, because of the surrounding pores, will have relatively high electrical resistance. As a result, this will cause high local Joule heat (or enhanced temperature gradient) in these local contact areas [19–21], resulting in severe local nano-crystallization as shown above. With a high applied pressure of 600 MPa, the combined effect of the pressure and the electrical discharge during SPS can effectively disrupt the oxide surface layers on the powder particles leading to a complete removal of the surface oxides. Without the oxide surface layers, viscous flow occurs making full densification possible. This eliminates overheated local areas and therefore prevents local nano-crystallization.

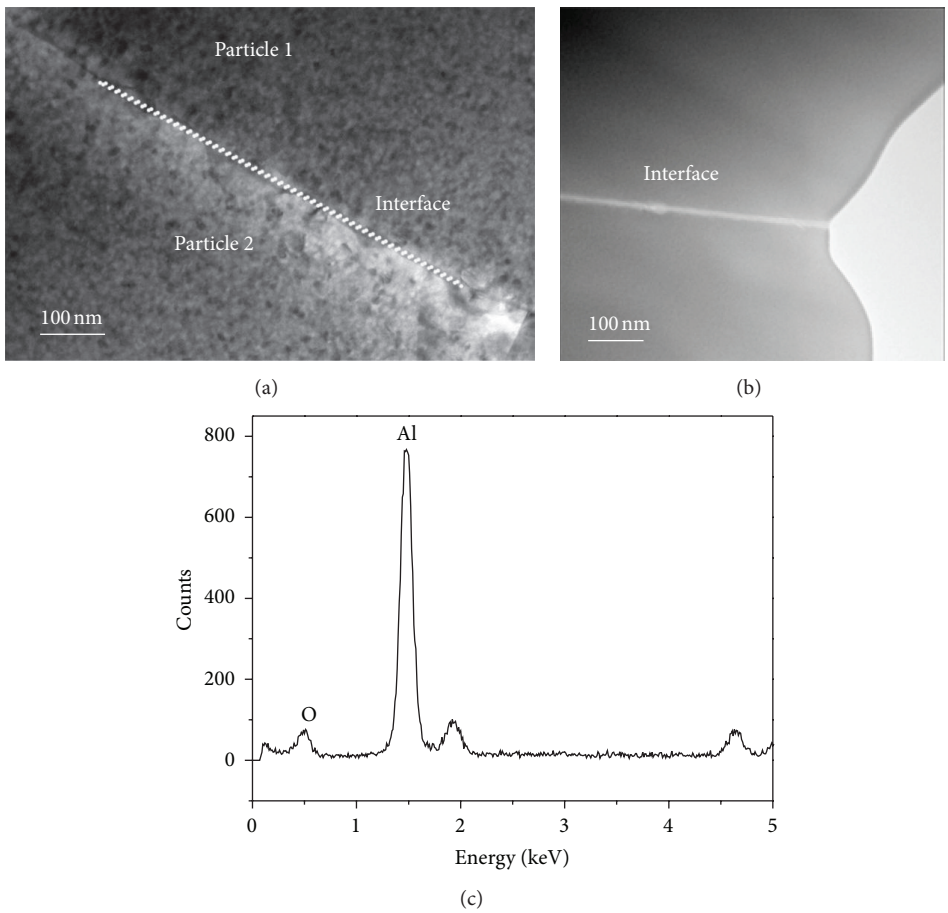

Figure 4: TEM bright field (BF) images of particle-particle interfaces in SPS-processed samples: (a) sintered at 248.5°C under 200 MPa; (b) sintered at 248.5°C under 600 MPa, free of crystallization; and (c) TEM-EDX results obtained from the interface shown in (a), indicative of noticeable crystallization of fcc-Al.

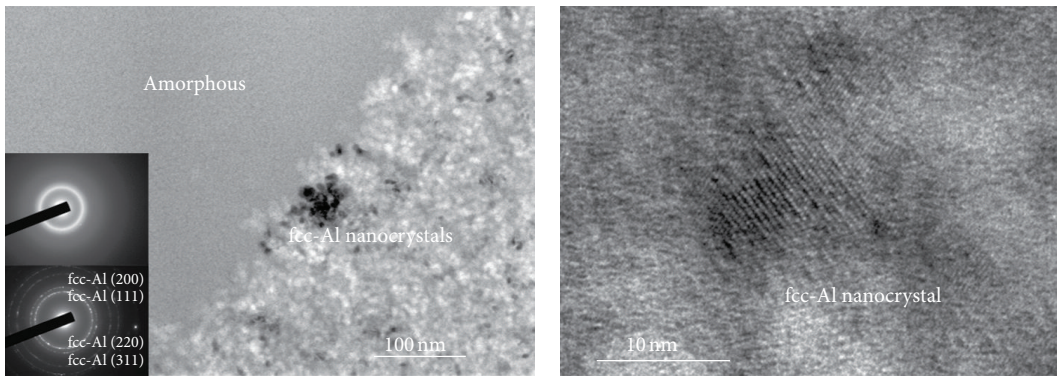

Figure 5: TEM BF image of an SPS-processed sample sintered at 248.5°C under 200 MPa. The inset in (a) is the corresponding SEAD patterns for the amorphous matrix and fcc-Al nanocrystals. (b) is an HRTEM image of the fcc-Al nanocrystals shown in (a).

4. Summary

$Al_{86}Ni_6Y_{4.5}Co_2La_{1.5}$ BMG disks (diameter: 10 mm; thickness: 4 mm) were fabricated from metallic glass powder of the same composition by SPS. The influence of applied pressure on the densification of $Al_{86}Ni_6Y_{4.5}Co_2La_{1.5}$ metallic glass powder was investigated at different sintering temperatures at a fixed heating rate of 40°C/min. Applying a high pressure (600 MPa) assisted in the removal of the surface oxide layers that enveloped the starting metallic glass powder. This led to full densification of the metallic glass powder flow free of particle-particle interface oxides and nano-crystallization.

The mechanism was attributed to potential viscous flow during SPS between the powder particles. In contrast, both residual oxides and nanocrystalline Al phases were detected at particle-particle interfaces in the $Al_{86}Ni_6Y_{4.5}Co_2La_{1.5}$ BMGs fabricated under a low pressure (200 MPa) with respect to the same heating and isothermal sintering parameters. The applied pressure showed a predominant influence on the removal of the surface oxide layers on the starting metallic glass powder during SPS, which is crucial to the consolidation of the metallic glass powder.

Acknowledgments

This work was supported by the Australian Research Council (ARC). The authors would like to thank Professor Jianqiang Wang of the Institute of Metal Research, Chinese Academy of Sciences, for the provision of the powder. M. Yan acknowledges supports from the Queensland Smart Future Fellowship Programme (Early Career) and a UQ Early Career Researcher Grant. The authors also acknowledge the assistance from the Centre for Microscopy and Microanalysis (CMM) of The University of Queensland and the Australian Microscopy & Microanalysis Research Facility (AMMRF).

References

[1] W. H. Wang, C. Dong, and C. H. Shek, "Bulk metallic glasses," *Materials Science and Engineering R*, vol. 44, no. 2-3, pp. 45–89, 2004.

[2] A. Inoue, "Amorphous, nanoquasicrystalline and nanocrystalline alloys in Al-based systems," *Progress in Materials Science*, vol. 43, no. 5, pp. 365–520, 1998.

[3] B. J. Yang, J. H. Yao, Y. S. Chao, J. Q. Wang, and E. Ma, "Developing aluminum-based bulk metallic glasses," *Philosophical Magazine*, vol. 90, no. 23, pp. 3215–3231, 2010.

[4] M. Yan, S. Kohara, J. Q. Wang, K. Nogita, G. B. Schaffer, and M. Qian, "The influence of topological structure on bulk glass formation in Al-based metallic glasses," *Scripta Materialia*, vol. 65, no. 9, pp. 755–758, 2011.

[5] M. Yan, J. Q. Wang, C. Kong, G. B. Schaffer, and M. Qian, "Micrometer-sized quasicrystals in the $Al_{85}Ni_5Y_6Co_2Fe_2$ metallic glass: a TEM study and a brief discussion on the formability of quasicrystals in bulk and marginal glass-forming alloys," *Journal of Materials Research*, vol. 27, no. 16, pp. 2131–2139, 2012.

[6] B. J. Yang, J. H. Yao, J. Zhang, H. W. Yang, J. Q. Wang, and E. Ma, "Al-rich bulk metallic glasses with plasticity and ultrahigh specific strength," *Scripta Materialia*, vol. 61, no. 4, pp. 423–426, 2009.

[7] A. Inoue, K. Ohtera, A. P. Tsai, and T. Masumoto, "Aluminum-based amorphous-alloys with tensile-strength above 980 Mpa, (100 Kg/Mm^2)," *Japanese Journal of Applied Physics Part 2*, vol. 27, no. 4, pp. L479–L482, 1988.

[8] X. P. Li, M. Yan, B. J. Yang, J. Q. Wang, G. B. Schaffer, and M. Qian, "Crystallization behaviour and thermal stability of two aluminium-based metallic glass powder materials," *Materials Science and Engineering A*, vol. 530, pp. 432–439, 2011.

[9] C. K. Kim, H. S. Lee, S. Y. Shin, J. C. Lee, D. H. Kim, and S. Lee, "Microstructure and mechanical properties of Cu-based bulk amorphous alloy billets fabricated by spark plasma sintering," *Materials Science and Engineering A*, vol. 406, no. 1-2, pp. 293–299, 2005.

[10] T. S. Kim, J. Y. Ryu, J. K. Lee, and J. C. Bae, "Synthesis of Cu-base/Ni-base amorphous powder composites," *Materials Science and Engineering A*, vol. 448-451, pp. 804–808, 2007.

[11] X. Li, A. Makino, H. Kato, A. Inoue, and T. Kubota, "$Fe_{76}Si_{9.6}B_{8.4}P_6$ glassy powder soft-magnetic cores with low core loss prepared by spark-plasma sintering," *Materials Science and Engineering B*, vol. 176, no. 15, pp. 1247–1250, 2011.

[12] D. J. Wang, Y. J. Huang, J. Shen, Y. Q. Wu, H. Huang, and J. Zou, "Temperature influence on sintering with concurrent crystallization behavior in Ti-based metallic glassy powders," *Materials Science and Engineering A*, vol. 527, no. 10-11, pp. 2662–2668, 2010.

[13] P. P. Choi, J. S. Kim, O. T. H. Nguyen, D. H. Kwon, Y. S. Kwon, and J. C. Kim, "Al-La-Ni-Fe bulk metallic glasses produced by mechanical alloying and spark-plasma sintering," *Materials Science and Engineering A*, vol. 448-451, pp. 1119–1122, 2007.

[14] T. T. Sasaki, K. Hono, J. Vierke, M. Wollgarten, and J. Banhart, "Bulk nanocrystalline $Al_{85}Ni_{10}La_5$ alloy fabricated by spark plasma sintering of atomized amorphous powders," *Materials Science and Engineering A*, vol. 490, no. 1-2, pp. 343–350, 2008.

[15] X. P. Li, M. Yan, H. Imai et al., "Fabrication of 10 mm diameter fully dense $Al_{86}Ni_6Y_{4.5}Co_2La_{1.5}$ bulk metallic glass with high fracture strength," *Materials Science and Engineering A*, vol. 568, pp. 155–159, 2013.

[16] M. Yan, P. Yu, K. B. Kim, J. K. Lee, G. B. Schaffer, and M. Qian, "The surface structure of gas-atomized metallic glass powders," *Scripta Materialia*, vol. 62, no. 5, pp. 266–269, 2010.

[17] X. P. Li, M. Yan, J. Q. Wang et al., "Non-isothermal crystallization kinetics and mechanical properties of $Al_{86}Ni_6Y_{4.5}Co_2La_{1.5}$ metallic glass powder," *Journal of Alloys and Compounds*, vol. 530, pp. 127–131, 2012.

[18] Z. A. Munir, U. Anselmi-Tamburini, and M. Ohyanagi, "The effect of electric field and pressure on the synthesis and consolidation of materials: a review of the spark plasma sintering method," *Journal of Materials Science*, vol. 41, no. 3, pp. 763–777, 2006.

[19] G. Ji, F. Bernard, S. Launois, and T. Grosdidier, "Processing conditions, microstructure and mechanical properties of hetero-nanostructured ODS FeAl alloys produced by spark plasma sintering," *Materials Science and Engineering A*, vol. 559, pp. 566–573, 2013.

[20] T. Grosdidier, G. Ji, and S. Launois, "Processing dense hetero-nanostructured metallic materials by spark plasma sintering," *Scripta Materialia*, vol. 57, no. 6, pp. 525–528, 2007.

[21] G. Ji, T. Grosdidier, N. Bozzolo, and S. Launois, "The mechanisms of microstructure formation in a nanostructured oxide dispersion strengthened FeAl alloy obtained by spark plasma sintering," *Intermetallics*, vol. 15, no. 2, pp. 108–118, 2007.